International Journal of Hyperthermia

ISSN: 0265-6736 (Print) 1464-5157 (Online) Journal homepage: www.tandfonline.com/journals/ihyt20

Generating and monitoring mild hyperthermia using a ring array ultrasound transducer

David Bustamante, Yan Yan, Trevor Mitcham, Rehman Ali, Brian Marples, Kimberly R. Gergelis, Peter Littrup, Nebojsa Duric & Mohammad Mehrmohammadi

To cite this article: David Bustamante, Yan Yan, Trevor Mitcham, Rehman Ali, Brian Marples, Kimberly R. Gergelis, Peter Littrup, Nebojsa Duric & Mohammad Mehrmohammadi (2024) Generating and monitoring mild hyperthermia using a ring array ultrasound transducer, International Journal of Hyperthermia, 41:1, 2376681, DOI: 10.1080/02656736.2024.2376681

To link to this article: https://doi.org/10.1080/02656736.2024.2376681

Published online: 07 Aug 2024.

INTERNATIONAL JOURNAL OF HYPERTHERMIA
2024, VOL. 41, NO. 1, 2376681
https://doi.org/10.1080/02656736.2024.2376681

Generating and monitoring mild hyperthermia using a ring array ultrasound transducer

David Bustamante[a], Yan Yan[b], Trevor Mitcham[b], Rehman Ali[b], Brian Marples[c], Kimberly R. Gergelis[c], Peter Littrup[a], Nebojsa Duric[a,b,d] and Mohammad Mehrmohammadi[a,b,d]

[a]Department of Biomedical Engineering, Hajim School of Engineering and Applied Sciences, University of Rochester, Rochester, New York, USA; [b]Department of Imaging Sciences, School of Medicine and Dentistry, University of Rochester Medical Center, Rochester, New York, USA; [c]Department of Radiation Oncology, School of Medicine and Dentistry, University of Rochester Medical Center, Rochester, New York, USA; [d]Department of Electrical and Computer Engineering, Hajim School of Engineering and Applied Sciences, University of Rochester, Rochester, New York, USA

ABSTRACT

Objective: To demonstrate the feasibility of using a ring array ultrasound (US) transducer, guided by ultrasound tomography (UST), for generating and monitoring mild hyperthermia (MHTh).

Methods: *In silico* and *in vitro* experiments were designed to evaluate the efficacy of a ring array US transducer for generating MHTh and monitoring changes in temperature. In a series of *in silico* studies, we compared the acoustic focal profiles produced by a ring array US transducer transmitting at different frequencies and further investigated the effectiveness of UST-guidance in implementing aberration correction to enhance the focal profile. *In vitro* experiments evaluated the capability of using a ring array US transducer to generate and maintain MHTh and the accuracy of using UST to monitor temperature changes.

Results: The simulations demonstrated that a ring array US transducer achieves symmetrical and localized acoustic focusing. In a heterogenous tissue model, a ring array US transducer achieved a superior acoustic focus by implementing aberration correction with guidance from UST. *In vitro* experiments demonstrated the capability of a ring array US transducer to generate MHTh in a tissue-mimicking phantom in an average of 117 ± 18 s and subsequently maintain MHTh. Lastly, a ring array US transducer utilized UST to track temperature changes in a preheated water-filled inclusion while it passively cooled from 45 °C to 25 °C, with a maximum error of 0.58 °C.

Conclusion: A ring array US transducer can noninvasively generate and monitor MHTh, overcoming many limitations of current clinical systems. The closed geometry of the transducer is optimal for acoustic focusing and UST-guidance allows for improved aberration correction in a heterogenous medium. Utilizing UST thermometry with the same ring array US transducer will allow for implementing an image-guided, temperature-controlled, all-acoustic MHTh system.

ARTICLE HISTORY
Received 15 April 2024
Revised 31 May 2024
Accepted 2 July 2024

KEYWORDS
Ultrasound; tomography; image-guided; mild hyperthermia; ring array transducer

1. Introduction

Mild hyperthermia (MHTh) is a therapeutic procedure where targeted tissue volumes are heated to slightly elevated temperatures (~43 °C or $\Delta T \leq 6$ °C), which has been shown to increase the efficacy of various cancer treatments such as chemo-, immuno-, and radiation therapy to improve tumor control [1–9]. Focused ultrasound (FUS) has been used to generate MHTh and is often used under MRI and US-guidance to control and monitor temperature [10–22]. Compared to noninvasive radiofrequency or microwave antenna-based MHTh systems, FUS achieves superior heat localization [12,13,15,20,23,24]. However, existing FUS techniques are limited by localized heat generation at higher tissue depths, especially when a single US probe is used [25–27]. Additionally, focusing acoustic waves in a heterogeneous medium is difficult because of acoustic aberrations, which are caused by acoustic waves traversing tissue layers with a different sound speed (SS). Conventional FUS systems typically are not able to effectively compensate for acoustic aberrations alone [28]. Current clinical systems require pretreatment planning images such as an X-ray CT scan and an MRI to compensate for acoustic aberrations. This introduces significant limitations, including more time, complexity, and cost, thereby reducing accessibility [29–31]. Furthermore, these image-guidance modalities cannot be performed during MR-guided FUS MHTh treatment concurrent with FUS heating and MR thermometry, which potentially limits their clinical utility for real-time phase-aberration correction.

A major challenge for the clinical implementation of current MHTH systems is noninvasively monitoring temperature with accuracy comparable to gold standard invasive

CONTACT Mohammad Mehrmohammadi mohammad_mehr@urmc.rochester.edu Department of Imaging Sciences, School of Medicine and Dentistry, University of Rochester Medical Center, 601 Elmwood Ave., Box 648, Rochester, NY 14642, USA

thermometry probes (± 0.1 °C) [1]. MRI thermometry is the clinical gold standard for noninvasive temperature monitoring during MHTh procedures, as it is capable of measuring both absolute temperature and temperature changes in large 3D volumes and at large depths. However, incorporating MRI thermometry for monitoring and guiding MHTh procedures has limitations including low temporal resolution, limited availability, higher cost, and added complexity because of the need to build the hyperthermia devices from non-magnetic components [14,32–34]. US offers the advantage of noninvasive thermometry, as it can measure temperature changes by evaluating changes in SS, which are directly related to temperature [13]. However, US thermometry has been practically limited in clinical application with transducers that utilize reflection mode acquisition. Main limiting factors include its inaccuracy due to acoustic aberrations (especially in heterogenous tissue), a limited field of view, the inability to monitor tissues surrounded by bone or air cavities, and the variability in echo time shifts caused by tissue deformation during heating [35–37]. In contrast, transmission mode UST with a ring array US transducer has been shown to generate accurate tissue SS maps, and thus provides an opportunity to accurately measure tissue temperature [13]. The capability of UST to provide accurate tissue composition maps, and in particular precise SS measurements, enables a noninvasive method for monitoring temperature during a MHTh procedure. Combining MHTh generation with the temperature monitoring capability of a ring array US transducer provides an opportunity for the first noninvasive all-acoustic system to generate and monitor MHTh [13,38].

These studies begin with numerical simulations to evaluate the importance of transducer geometry on acoustic focusing, assessing the focusing of a ring array US transducer operating at different frequencies. Later studies evaluate the efficacy of accounting for acoustic aberrations in a heterogeneous media against a model that assumes a uniform SS using a ring array US transducer. Subsequently, two *in vitro* studies used ring array US transducers to demonstrate their capability to use FUS to generate MHTh and to use UST to monitor temperature changes. Our objective is to demonstrate that utilizing FUS and UST with a ring array US transducer is an optimal solution to noninvasively generate and monitor MHTh. The ring array US transducers in this study are FDA-approved for breast cancer screening and diagnostic applications [39], which indicates the potential for clinical translation of the proposed theranostic system.

2. Materials and methods

2.1. Efficacy of acoustic focusing using a ring array transducer: in silico studies

In silico studies and data analyses were done using k-Wave toolbox and MATLAB® [40]. The aim of these simulations was to quantify the acoustic focusing capabilities of a ring array US transducer at different frequencies. Two 2D simulations were performed in a homogeneous medium with a fixed SS of 1540 m/s. The medium was specified with a spatial resolution of 50 µm, constant mass density of 1.1 g/cm^3, and was defined as lossless for simple comparison. The ring array US transducer's diameter was 22 cm containing 256 elements and width of 1.6 mm, which was used in previous imaging studies [38]. In the first simulation, the ring array US transducer operated at a lower transmit center frequency of 0.5 MHz (the lower limit of bandwidth in our existing hardware). For the second simulation, it operated at 1.5 MHz. In each scenario, a sinusoidal pressure wave was focused on the center of the grid and the subsequent maximum pressure in the grid was recorded. To ease comparison, the pressure profiles were normalized based on the global maximum pressure in the two simulations.

2.2. UST-assisted aberration correction: in silico studies

This set of *in silico* studies aimed to evaluate the efficacy of implementing aberration correction using a ring array US transducer within a heterogeneous medium, as opposed to assuming a uniform SS. Aberration correction was implemented by utilizing UST-acquired SS maps integrated into time-reversal (TR) focusing. TR functions by inverting the time delays captured at each transducer, which are affected by tissue SS and transducer geometry, and subsequently retransmitting the time-reversed signals [41–43] to focus acoustic waves. TR focusing through a heterogeneous medium is challenging and can be inaccurate due to aberrations caused by non-uniform acoustic properties of tissues, including SS and acoustic attenuation (AA) [43–46]. A ring array US transducer can more effectively utilize TR focusing to implement aberration correction because UST acquires high resolution SS and AA images [44].

TR focusing was applied in simulations using a 256-element ring array US transducer surrounding a numerical breast phantom that was acquired from a real patient breast UST dataset [40], consisting of fat, fibroglandular tissues, and surrounding water. A dense breast phantom containing a lesion was chosen for this study because it is a highly scattering medium, for which advanced MR-guided FUS systems have significant difficulties in accurate acoustic focusing [47–51]. The ring array US transducer used a 0.5 MHz transmission center frequency. The grid had a spatial resolution of 250 µm. The acoustic focus was placed in the middle of a tumor (3' o clock) identified by an unusually high SS. In one simulation, TR focusing was applied with an assumed uniform SS and AA value equal to the averages of the medium (fat, fibroglandular, and water at 37 °C). In a second simulation, the spatial SS and AA maps were used to create aberration-corrected TR focusing.

A second similar set of simulations was designed for the purpose of evaluating the effect of applying UST-driven aberration correction in a simplified scenario with more aberrations present, utilizing a circular numerical breast-mimicking phantom. The phantom featured a 50 mm-thick layer of fibroglandular (FG) tissue encased in a 100 mm-thick fat layer (150 mm total diameter). The focus was set off-center at the FG-fat interface (50 mm deep) to validate that accurate focusing does not depend on tissue symmetry. Similar to the previous simulations, two simulated scenarios were compared: (1) TR focusing was applied with an assumed uniform SS and AA value throughout the medium, and (2) the spatial SS and AA maps were used to create aberration-corrected TR focusing. For all simulations, the normalized maximum pressure profiles were recorded, and the efficacy of aberration correction was quantified based on the location and intensity of the achieved focal point.

2.3. MHTh generation and maintenance with a ring array transducer

To evaluate the efficacy of using a 256-element ring array US transducer to generate the heating requisite for MHTh, a cylindrical phantom with a diameter of 10 cm and height of 5 cm was made out of polyvinyl chloride (PVC, M-F Manufacturing Co. Fort Worth, TX, USA) according to the protocol described in [52]. The SS of PVC is 1400 m/s. A 3 mm diameter hole (2 cm depth) was created at the center of the PVC phantom. PVC was chosen because it has a density and acoustic parameters close to water and has significant thermal isolation, which limited the systemic error from heat diffusion [53,54]. The phantom was placed in the center of the ring array and coupled to it with deionized room temperature (18.8 °C) water. The central hole in the phantom was also filled with deionized room temperature water (0.014 ml). Before generating MHTh, a needle hydrophone (HNA-0400, ONDA Corporation, Sunnyvale, California) was inserted and recorded the maximum pressure. Subsequently, the hydrophone was substituted for an ultrathin (200 µm diameter with accuracy of ± 0.2 °C) optical thermometer (TS2, WEIDMANN OPTOCON, Dresden, Germany) to record the temperature during heating. To generate heat, all elements were driven simultaneously at 1.5 MHz (center frequency of the ring) at 33% maximum possible acoustic power (acoustic output is ~20 kPa per element) and 0.5% duty cycle. This low duty cycle was chosen to demonstrate the minimal power requirement necessary to generate the required heat for MHTh and was empirically found to be ideal for heating to the target in about 2 min (~3 °C increase per min). These measurements were repeated 3 times with starting temperatures of 18.8, 19.1, and 19.6 °C. In each case, the temperature was increased by 6 °C (the maximum accepted ΔT for clinical MHTh applications) and then maintained within 6 ± 0.1 °C for 5 min by gradually decreasing the acoustic output through decreasing the elements' driving voltages. A passive cooling period of 20 min between each heating trial was allotted to allow the phantom to cool back to room temperature.

2.4. UST thermometry with a ring array transducer

It is well known that there is a direct relationship between the temperature and SS of tissues [55–57]. This relationship allows SS images to be converted to temperature images with prior information of the tissue's composition, which can be acquired with UST [58–61]. To evaluate the efficacy of utilizing UST with a ring array US transducer to monitor changes in temperature, an experiment was designed by creating a cylindrical phantom with a diameter of 10 cm and a height of 8 cm, made out of porcine gelatin (8% w/v) according to the protocol described in [62]. Gelatin was utilized since the acoustic properties are close to that of soft tissues [63]. The SS of the gelatin material is 1502 m/s. Two cylindrical holes with a diameter of 25 mm, separated by 20 mm, were created in the gelatin. To prevent the phantom from melting due to the preheated water, 0.1 ml (0.0002% w/v) glutaraldehyde was added during preparation. Once the phantom was made, one of the holes was filled with water preheated to 47 °C, and the second hole was filled with room temperature water to serve as reference in UST measurements. The same optical thermometer was used to measure the water temperature during cooling while synchronous UST measurements of the phantom were acquired. UST images were acquired every 1–2 °C drop starting at 45 °C (after the initial rapid cooling stablized) with a 1024-element ring array US transducer until the water passively cooled to room temperature in ~17 minutes from the initial to final acquisition. A 1024-element ring array was used because using more elements results in better resolution and accuracy, at the cost of increasing computation time. The 1024-element ring array has a center frequency of 3 MHz, but the transmission center frequency was set at 700 kHz to avoid cycle skipping reconstruction errors at lower frequencies. The SS images were synthesized in post-processing using a full waveform inversion (FWI) algorithm to achieve optimal accuracy on an NVIDIA 4090 GPU [64,65]. SS images were converted to temperature using an established 5th order polynomial for water to create UST-driven temperature images [59]. SS measurements (and corresponding temperature maps) acquired at different temperatures within the heated water inclusion were analyzed by segmenting a circular 1 cm region of interest (ROI) in the center of the inclusion and the mean and standard deviation of the pixels were calculated. This inner 1 cm circle was selected instead of the full diameter because heat accumulates along the edges of the hole, whereas it is more homogenous in the inner 1 cm circle where the optical thermometer was inserted for reference temperature recordings. The change in SS between consecutive acquisitions was calculated and compared to the expected values from literature.

3. Results

3.1. Enhanced acoustic focusing using a ring array US transducer

In these simulations, we evaluated a ring array's acoustic focal profile at two frequencies. Figure 1 compares the normalized pressure profiles at 0.5 (Figure 1a) and 1.5 MHz (Figure 1b). At 0.5 MHz, the ring array US transducer achieved an acoustic focus of 1.6 mm × 1.6 mm (lateral full width at half maximum (FWHM) × axial FWHM). At 1.5 MHz, the FWHM was 0.5 × 0.5 mm.

3.2. Effect of aberration correction on the acoustic focus

A real patient UST breast image correction (Figure 2a) was used to assess the efficacy of applying aberration correction. Figure 2b shows the beam profile when an averaged SS and AA was uniformly assigned throughout the medium (no aberration correction). The pressure was spatially distorted and significantly less localized in contrast to Figure 2c, which implements aberration correction. The second set of simulations with a simplified breast model (Figure 2d) demonstrated similar behavior. When a uniform SS and AA is assigned to the medium, the focal point was shifted from its targeted location by 1.7 mm, and the maximum acoustic intensity was reduced from 1 MPa to 0.92 MPa, and the pressure localization was significantly improved by implementing aberration correction. The FWHMs were 2.75 mm (horizontal – x axis) and 3 mm (vertical - y axis) without aberration correction (Figure 2e) and improved to a symmetrical 2 mm × 2 mm after aberration correction (Figure 2f).

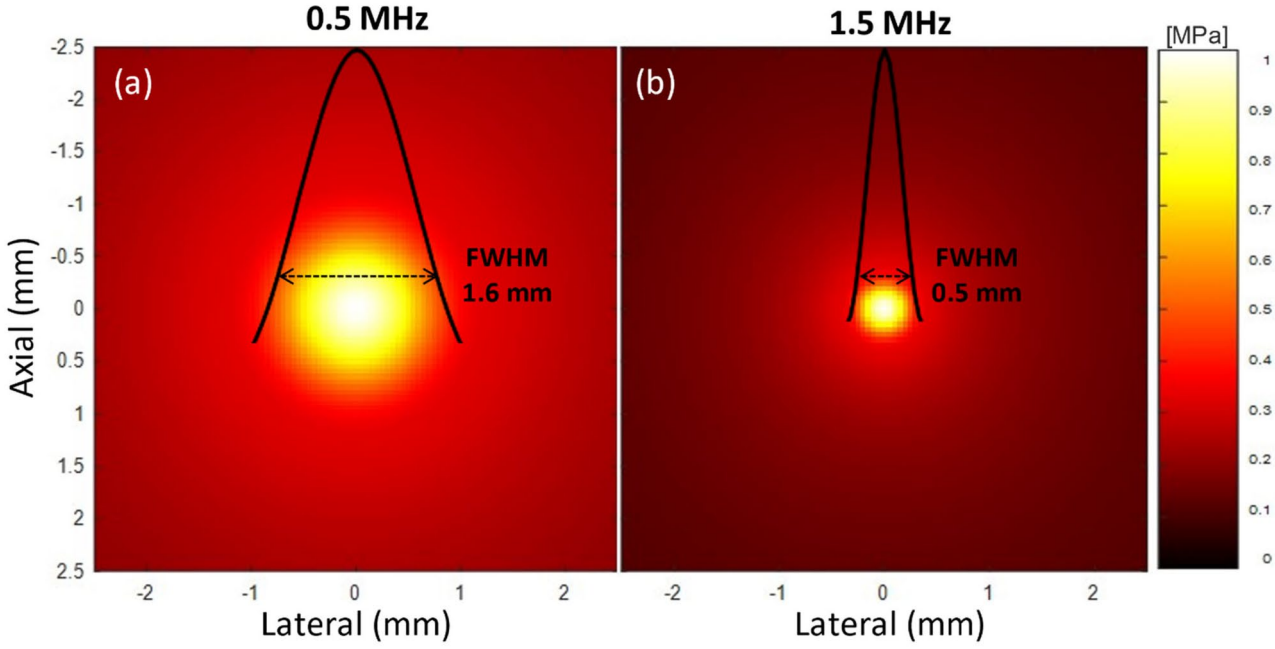

Figure 1. Symmetric and localized acoustic focal profile of a ring array US transducer. 256-element ring array US transducer's focal profile with overlaid pressure curve at (a) 0.5 MHz and (b) at 1.5 MHz. Pressure profiles were normalized and are shown in the Central −2.5 to 2.5 mm portion of the grid. Lateral FWHM (indicated by dashed black arrows) is equivalent to axial FWHM (not shown) at both frequencies.

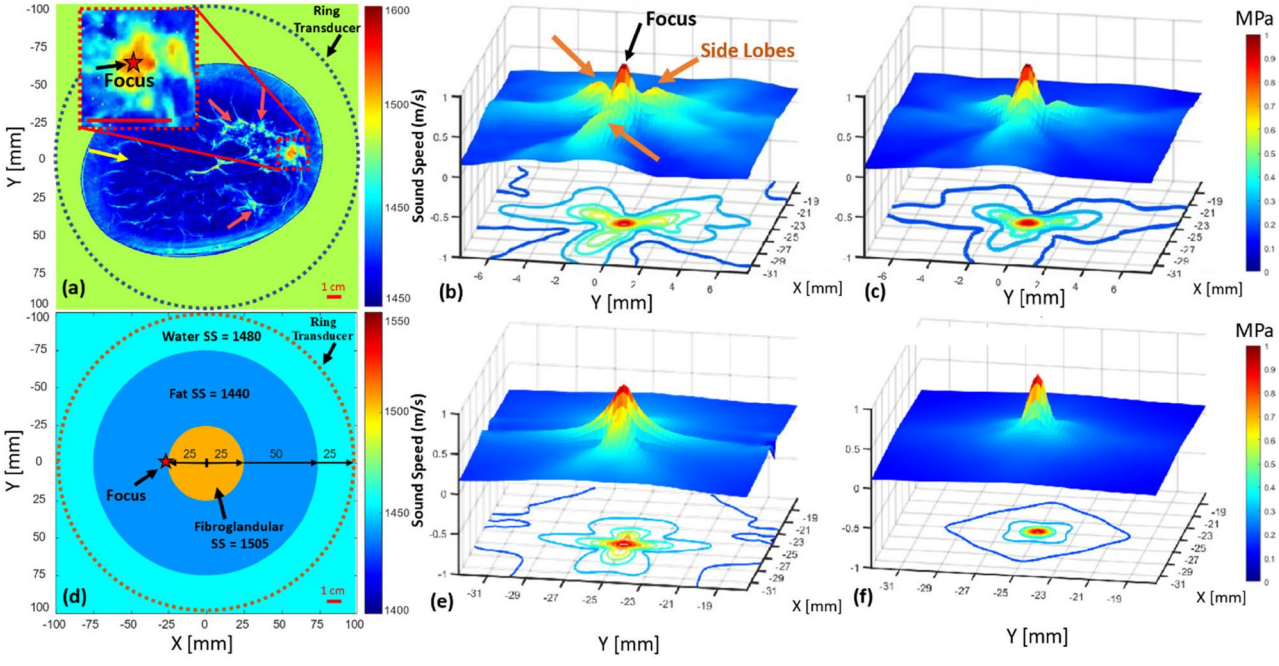

Figure 2. UST-assisted TR focusing significantly improves the acoustic focal profile in a heterogeneous medium. (a) real patient clinical UST breast image consisting of a tumor (the focus), fat, FG, and surrounding water. (b) acoustic focal profile without aberration correction. The black arrow indicates the peak acoustic pressure. Orange arrows indicate the side lobes. (c) acoustic focal profile with aberration correction. The side lobes are significantly reduced. (d) simplified circular numerical breast model with a focus point placed on the intersection of the fat and FG tissue. (e) acoustic focal profile without aberration correction. The peak acoustic pressure is reduced and shifted from its target point. (f) acoustic focal profile with aberration correction.

3.3. Generating and maintaining MHTh with a ring array transducer

To generate heat, focused transmission was maintained until the temperature in the center of the phantom increased by 6 °C in three trials (Figure 3, one trial). An average time of 117 ± 18 s was required to heat the target by 6 °C. Additionally, a maximum focal pressure of 800 kPa (peak negative pressure) was recorded. This corresponds to mechanical index (MI) of 0.65, which is significantly below

the risk of adverse bioeffects such as cavitation (MI <1.9 is the FDA recommendation for diagnostic devices) [66]. For reference, in standard MHTh treatment, where the target temperature typically does not exceed 43 °C [2–4, 67], peak pressure typically ranges from 1 to 3 MPa (max intensity 10–100 W/cm^2) depending on the desired rate of heating [8, 10, 12, 24, 67,68].

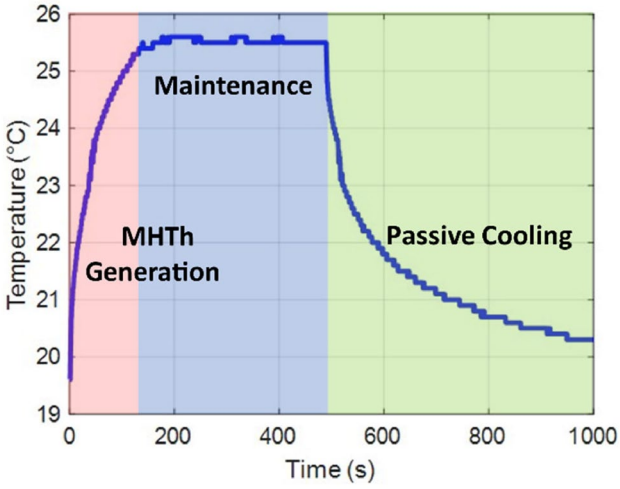

Figure 3. Generating and maintaining MHTh with a ring array in the center of a 10 cm thick PVC phantom. The figure is the temperature from one trial recorded by the optical thermometer. The rate of generating MHTh and subsequent maintenance was similar in all three trials.

3.4. Monitoring temperature using UST with a ring array US transducer

In this experiment, changes in temperature were analyzed based on SS images (Figure 4a–e) and corresponding temperature images (Figure 4f–j) and compared to the expected values from literature. The measured SS changes were plotted against the temperature recorded by the optical thermometer (Figure 4k). For display, the reference ΔSS (ΔSS = 0) was set to align with a temperature of 37 °C. The measured SS changes had a high correlation (R^2 = 0.99) with literature reported values with an absolute error of less than 1%. In the temperature images, the mean error (difference between UST-driven temperature mean values and optical thermometer values) was 0.06 ± 0.26 °C (maximum positive error was +0.53 °C, maximum negative error was −0.58 °C).

4. Discussion

4.1. Enhanced acoustic focusing using a ring array US transducer

Focusing acoustic energy in tissues has been widely studied for different transducer geometries [41,42]. This study demonstrated the efficacy of using a ring array transducer geometry for precise acoustic focusing. Based on these results, a ring array US transducer has better focusing capabilities than conventional clinical transducers, as well as current HIFU systems that are utilized for MHTh [15,20,21]. In the context of clinical MHTh, this precise focusing may be

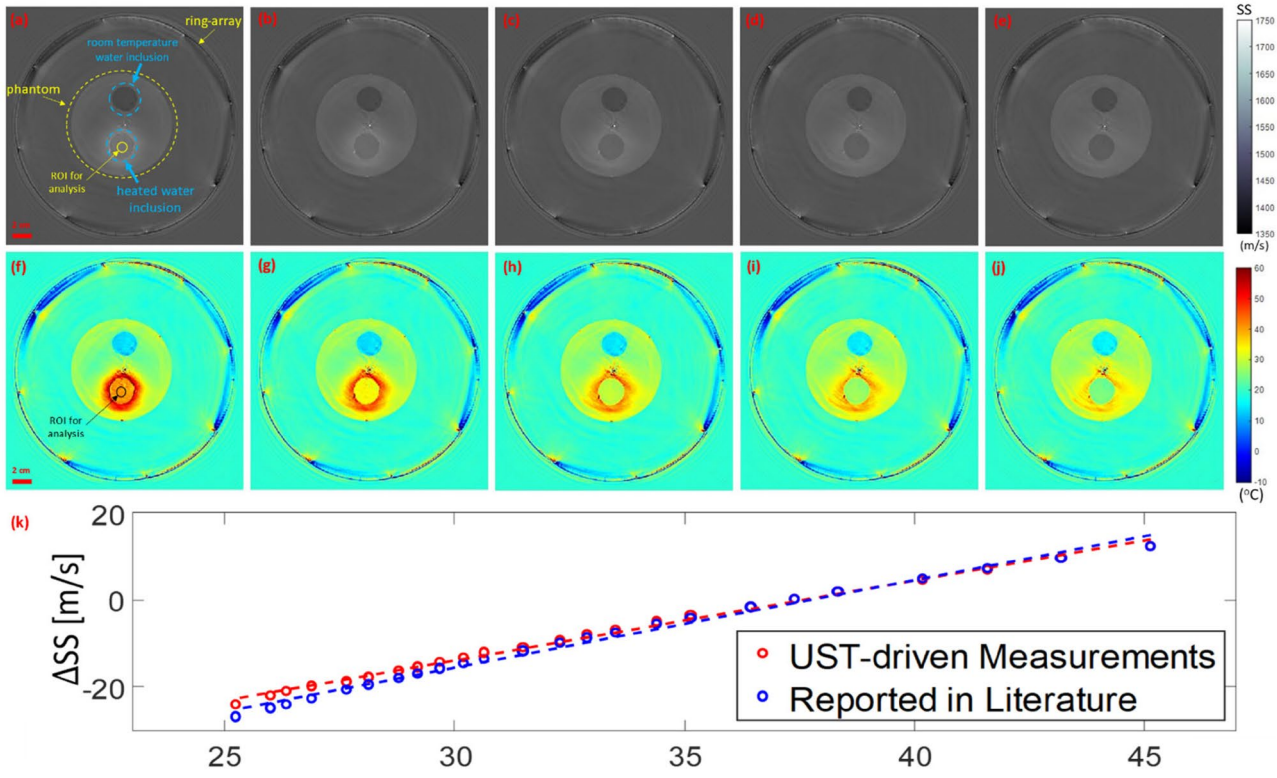

Figure 4. UST can accurately monitor changes in temperature. (a-e) SS images acquired during passive cooling, including the first UST image (a) and the final image (e), and 3 evenly spaced acquisitions. (f-j) corresponding UST-driven temperature images, (k) change in SS for each consecutive acquisition (red) and the expected change in SS from literature (blue) versus the optical thermometer recorded temperature values (horizontal axis).

important for several reasons, such as targeting complex-shaped tumors, focusing on tumors in deep tissues, or to target (or avoid) blood vessels.

4.2. Effect of aberration correction on the acoustic focus

With the typical assumption of uniform acoustic properties for a heterogenous medium, the acoustic focal profile is both spatially shifted and distorted, a problem that UST-guided TR can overcome [42,69]. Our simulations demonstrated that aberration correction resulted in a more localized focal spot (Figure 2c and f - reduced lobes), which indicates the potential for a highly targeted and localized heating by using UST-assisted aberration correction. These results demonstrated that acoustic aberrations have a significant effect on focusing acoustic waves in deep tissues, and the closed geometry of the ring array is optimal for implementing aberration correction.

4.3. Generating and maintaining MHTh with a ring array transducer

MHTh was reached in average of less than 2 min, which is significantly faster than most other noninvasive and non-US modalities, which typically require 15 – 30 min to reach the target temperature safely [2,4,67]. This was done at a pressure that was low enough to avoid any risk of cavitation (MI = 0.65), which validates the efficacy of the system for rapidly generating heat while posing minimal risk. Given this low MI, it is anticipated that a ring array US transducer can generate heat at a significantly faster rate with minimal risk by increasing the duty cycle or the acoustic output. Furthermore, while this study aimed to demonstrate the generation and maintenance of MHTh in a relatively small target, the ring array system is capable of heating larger volumes by using sequential heating, where the focus point can be moved to cover larger volumes, which was demonstrated in our previous study [13].

4.4. Monitoring temperature using UST with a ring array US transducer

While this study demonstrated a high correlation between the SS changes and temperature changes, the initial average SS in the inclusion (Figure 4a) was 1529.9 m/s (corresponding to a temperature of 40.6 °C, Figure 4f) and the final average SS in the cooled down inclusion was 1493.0 m/s (corresponding to a temperature of 23.7 °C, Figure 4j). These values show an offset from the optical thermometer measurements, which could be minimized through a set of calibration studies. Multiple factors may contribute to this offset, including a small delay between optical sensor measurements and UST acquisition, necessitating precise synchronization and faster acquisition. These factors are the subjects of our ongoing studies. Nevertheless, the high correlation between ΔT and ΔSS indicates the ease of calibrating the system at a single reference temperature or across a range of reference temperatures, thereby enabling measuring absolute temperature with high accuracy. Our results demonstrated that UST with a ring array is able to track temperature changes (ΔT) with better accuracy compared to other noninvasive modalities such as MRI thermometry [14]. While both the background and heated water inclusion in these experiments follow a similar incremental trend with increased temperature, fat and fat-based tissues are known to have opposite trends in temperature-dependent SS variations [70]. Therefore, synthesizing temperature maps from SS maps can only be done with prior information of tissue composition. However, given that UST has been demonstrated to be capable of acquiring accurate tissue composition maps with a ring array US transducer [39], this system provides an ideal platform for UST thermometry.

4.5. Combining cyclic heating with UST thermometry on a ring array to generate and monitor MHTh

Recently, the FDA approved UST for screening women with dense breast tissue, which has been evaluated with a ring array system in clinical studies [39]. The system was developed as an operator-independent volumetric breast cancer diagnostic imaging modality. However, this system has not yet been evaluated for its therapeutic potential. By implementing FUS on a ring array transducer system, as demonstrated in this study, it is possible to generate localized low intensity pressure fields, without risk of adverse bioeffects, and subsequently generate heat at rate ideal and safe for MHTh (1 - 3 °C per min). Based on these studies, it is envisioned that a ring array US transducer can combine the utility of FUS for generating MHTh and UST for monitoring temperature in an interleaved manner based on its ability to rapidly generate heat under UST guidance. The rapid generation of MHTh was accomplished at a precise focal point with a low-pressure and duty cycle, both of which could be increased to compensate for interleaved UST imaging. In these studies, temperature was measured by thermometer and was used as feedback to maintain the target temperature. Given the accuracy of UST-driven temperature measurements, it is envisioned that a UST-guided system will utilize UST thermometry as feedback to control and maintain MHTh during treatment. Combining UST with MHTh to generate a fully image-guided and temperature monitored MHTh system is the subject of our ongoing studies.

4.6. Implementing real-time temperature monitoring

In this study, the image reconstruction was done in post-processing, where every image was independently synthesized. While the goal was to assess the efficacy of using UST to track temperature changes and quantify its accuracy, the technique needs to be applied in real-time to be clinically relevant. We anticipate that the image reconstruction in future studies can be implemented with satisfactory frame rates of at least 1 frame per second, and thus interleaved with active-mode therapy, for three main reasons. First, a high-quality UST image can be acquired prior to the MHTh procedure in about 3 min (with 1024 elements), which can be used as a starting model in the FWI algorithm and can be updated every several seconds (< 5 s with our current resources). Second, the number of elements being used for imaging can be down sampled, while still maintaining high accuracy. For example, instead of using 1024 elements, 256 elements can be used (down sampled by 4x), which will accelerate image reconstruction. Third, computational power is becoming increasingly faster, and at much lower cost. In

the last five years, advancements in GPU technology have accelerated the potential reconstruction times of FWI algorithms by nearly an order of magnitude. In our future studies, we will assess the optimization of these factors for implementing real-time image reconstruction to monitor temperature. Additionally, alternative faster methods to FWI, such as ray-based methods, need to also be assessed and compared with FWI to determine their viability for monitoring temperature changes accurately during MHTh procedures.

5. Limitations

There were several limitations in this study that need to be addressed in future studies.

First, heating in this study was performed with a 256-element ring array instead of a 1024-element ring array because the accessible hardware was only capable of simultaneously driving 256 elements at a time. Utilizing more elements for heating may increase the efficiency and speed of the system.

Second, we used a simplified *in vitro* model with acoustic properties that mimic soft breast tissue for the purpose of assessing the high potential efficacy of using UST to track temperature changes. Therefore, the presented methods may not be directly applied to other models that include material beyond soft tissues, such as bone, without further tuning and calibrations. Given the accuracy level (<1% error) demonstrated in this study, a goal of future studies is to achieve similar accuracy for temperature tracking in *ex vivo* phantoms and *in vivo*.

Third, the entirety of the temperature images were synthesized by applying an algorithm that converts the SS of water to temperature. Therefore, the remainder of the temperature image, including the gelatin phantom, cannot be considered for accurate quantification of temperature. In future studies, the algorithm needs to consider individual material properties relating SS and temperature for synthesizing temperature images.

Fourth, the capability of UST to monitor temperature changes was implemented during cooling instead of during heating. Future studies need to demonstrate the capability of the system to interleave active-mode heating and UST imaging, which will require additional consideration and optimization for computational constraints, as well as potential biological effects, such as thermal expansion of tissues.

Lastly, future studies should assess the capability of the system to adjust the heating protocol based on thermometry feedback to account for uneven heating due to blood flow, which will be a challenge introduced with *in vivo* models.

6. Conclusion

These studies demonstrated the feasibility of using a ring array US transducer to generate and monitor MHTh. The geometry of a ring array US transducer is optimal for focusing acoustic pressure and implementing aberration correction. A ring array US transducer can rapidly and safely generate and maintain MHTh and can accurately monitor changes in temperature. By combining these functionalities, we anticipate that a ring array US transducer has the potential to be the first all-acoustic image-guided MHTh system.

Acknowledgements

The authors would like to thank Alexander Pattyn and Karl Kratkiewicz for their previous contributions towards developing this system. The authors also thank Kevin Parker for his insight into using the ring array system for generating mild hyperthermia.

Disclosure statement

Two of the authors, Nebojsa Duric and Peter Littrup, are co-founders and have financial interests in Delphinus Medical Technologies, which created the commercial FDA-approved ring array US transducer used for diagnostic breast imaging.

Funding

This work was partially supported by DOD-CDMRP Breakthrough Award (W81XWH-18-1-0039), and by the Richard Barber Interdisciplinary Research Funding Award from Wayne State University.

ORCID

David Bustamante http://orcid.org/0000-0002-6431-5859
Yan Yan http://orcid.org/0000-0001-8137-2372
Trevor Mitcham http://orcid.org/0000-0001-6985-5486
Rehman Ali http://orcid.org/0000-0003-2168-7895
Brian Marples http://orcid.org/0000-0002-8684-4372
Kimberly R. Gergelis http://orcid.org/0000-0002-8130-8327
Peter Littrup http://orcid.org/0000-0002-7760-2988
Nebojsa Duric http://orcid.org/0000-0001-6388-6863
Mohammad Mehrmohammadi http://orcid.org/0000-0002-9264-9354

Data availability statement

Data will be made available upon reasonable request to the corresponding author.

References

[1] Adibzadeh F, Sumser K, Curto S, et al. Systematic review of pre-clinical and clinical devices for magnetic resonance-guided radiofrequency hyperthermia. Int J Hyperthermia. 2020;37(1):15–27. doi:10.1080/02656736.2019.1705404.
[2] Ceelen W, Demuytere J, de Hingh I. Hyperthermic intraperitoneal chemotherapy: a critical review (in eng). Cancers (Basel). 2021;13(13):3114. doi:10.3390/cancers13133114.
[3] Crezee J, Franken NAP, Oei AL. Hyperthermia-based anti-cancer treatments (in eng). Cancers (Basel). 2021;13(6):1240. doi:10.3390/cancers13061240.
[4] Institute NC. Hyperthermia to treat cancer. 2024. [accessed April 01, 2024]. https://www.cancer.gov/about-cancer/treatment/types/hyperthermia.
[5] Takemoto M, Kuroda M, Urano M, et al. The effect of various chemotherapeutic agents given with mild hyperthermia on different types of tumours. Int J Hyperthermia. 2003;19(2):193–203. doi:10.1080/0265673021000035235.
[6] Ahmed K, Tabuchi Y, Kondo T. Hyperthermia: an effective strategy to induce apoptosis in cancer cells. Apoptosis. 2015;20(11):1411–1419. doi:10.1007/s10495-015-1168-3.
[7] Wust P, Hildebrandt B, Sreenivasa G, et al. Hyperthermia in combined treatment of cancer. Lancet Oncol. 2002;3(8):487–497. doi:10.1016/s1470-2045(02)00818-5.
[8] Toraya-Brown S, Fiering S. Local tumour hyperthermia as immunotherapy for metastatic cancer. Int J Hyperthermia. 2014;30(8):531–539. doi:10.3109/02656736.2014.968640.

[9] Overgaard J. The current and potential role of hyperthermia in radiotherapy. Int J Radiat Oncol Biol Phys. 1989;16(3):535–549. doi:10.1016/0360-3016(89)90470-7.
[10] Cho C-W, Liu Y, Cobb WN, et al. Ultrasound-induced mild hyperthermia as a novel approach to increase drug uptake in brain microvessel endothelial cells (in eng). Pharm Res. 2002;19(8):1123–1129. doi:10.1023/a:1019837923906.
[11] Shaw C, Ter Haar G, Rivens I, et al. Pathophysiological mechanisms of high-intensity focused ultrasound-mediated vascular occlusion and relevance to non-invasive fetal surgery. J R Soc Interface. 2014;11(95):20140029. doi:10.1098/rsif.2014.0029.
[12] Copelan A, Hartman J, Chehab M, et al. High-intensity focused ultrasound: current status for image-guided therapy (in eng). Semin Intervent Radiol. 2015;32(4):398–415. doi:10.1055/s-0035-1564793.
[13] Pattyn A, Kratkiewicz K, Alijabbari N, et al. Feasibility of ultrasound tomography–guided localized mild hyperthermia using a ring transducer: ex vivo and in silico studies. Med Phys. 2022;49(9):6120–6136. doi:10.1002/mp.15829.
[14] Rieke V, Butts Pauly K. MR thermometry (in eng). J Magn Reson Imaging. 2008;27(2):376–390. doi:10.1002/jmri.21265.
[15] Karzova MM, Kreider W, Partanen A, et al. Comparative characterization of nonlinear ultrasound fields generated by sonalleve v1 and v2 MR-HIFU systems. IEEE Trans Ultrason Ferroelectr Freq Control. 2023;70(6):521–537. doi:10.1109/TUFFC.2023.3261420.
[16] Tillander M, Hokland S, Koskela J, et al. High intensity focused ultrasound induced in vivo large volume hyperthermia under 3D MRI temperature control. Med Phys. 2016;43(3):1539–1549. doi:10.1118/1.4942378.
[17] Salomir R, Vimeux FC, de Zwart JA, et al. Hyperthermia by MR-guided focused ultrasound: accurate temperature control based on fast MRI and a physical model of local energy deposition and heat conduction. Magn Reson Med. 2000;43(3):342–347. doi:10.1002/(SICI)1522-2594(200003)43:3<342::AID-MRM4>3.0.CO;2-6.
[18] Pichardo S, Köhler M, Lee J, et al. In vivo optimisation study for multi-baseline MR-based thermometry in the context of hyperthermia using MR-guided high intensity focused ultrasound for head and neck applications. Int J Hyperthermia. 2014;30(8):579–592. doi :10.3109/02656736.2014.981299.
[19] Staruch R, Chopra R, Hynynen K. Localised drug release using MRI-controlled focused ultrasound hyperthermia. Int J Hyperthermia. 2011;27(2):156–171. doi:10.3109/02656736.2010.518198.
[20] Lennon JC, Hassan I. Magnetic resonance-guided focused ultrasound for Parkinson's disease since ExAblate, 2016–2019: a systematic review. Neurol Sci. 2021;42(2):553–563. doi:10.1007/s10072-020-05020-1.
[21] Siedek F, Yeo SY, Heijman E, et al. Magnetic resonance-guided high-intensity focused ultrasound (MR-HIFU): technical background and overview of current clinical applications (Part 1). Rofo. 2019;191(6):522–530. doi:10.1055/a-0817-5645.
[22] Sebeke L, Deenen DA, Maljaars E, et al. Model predictive control for MR-HIFU-mediated, uniform hyperthermia. Int J Hyperth. 2019;36(1):1039–1049. doi:10.1080/02656736.2019.1668065.
[23] Mulder HT, Curto S, Paulides MM, et al. Systematic quality assurance of the BSD2000-3D MR-compatible hyperthermia applicator performance using MR temperature imaging (in eng). Int J Hyperthermia. 2018;35(1):305–313. doi:10.1080/02656736.2018.1497209.
[24] Zhou YF. High intensity focused ultrasound in clinical tumor ablation (in eng). World J Clin Oncol. 2011;2(1):8–27. doi:10.5306/wjco.v2.i1.8.
[25] ter Haar G, Coussios C. High intensity focused ultrasound: physical principles and devices. Int J Hyperthermia. 2007;23(2):89–104. doi:10.1080/02656730601186138.
[26] Ter Haar G. HIFU tissue ablation: concept and devices. Adv Exp Med Biol. 2016;880:3–20. doi:10.1007/978-3-319-22536-4_1.
[27] Izadifar Z, Izadifar Z, Chapman D, et al. An introduction to high intensity focused ultrasound: systematic review on principles, devices, and clinical applications. J Clin Med. 2020;9(2):460. doi:10.3390/jcm9020460.
[28] Ali R, Brevett T, Zhuang L, et al. Aberration correction in diagnostic ultrasound: a review of the prior field and current directions. Z Med Phys. 2023;33(3):267–291. doi:10.1016/j.zemedi.2023.01.003.
[29] Ghanouni P, Pauly KB, Elias WJ, et al. Transcranial MRI-guided focused ultrasound: a review of the technologic and neurologic applications (in eng). AJR Am J Roentgenol. 2015;205(1):150–159. doi:10.2214/ajr.14.13632.
[30] Clement GT, Hynynen K. A non-invasive method for focusing ultrasound through the human skull (in eng). Phys Med Biol. 2002;47(8):1219–1236. doi:10.1088/0031-9155/47/8/301.
[31] Meng Y, Hynynen K, Lipsman N. Applications of focused ultrasound in the brain: from thermoablation to drug delivery. Nat Rev Neurol. 2021;17(1):7–22. doi:10.1038/s41582-020-00418-z.
[32] Fite BZ, Liu Y, Kruse DE, et al. Magnetic resonance thermometry at 7T for real-time monitoring and correction of ultrasound induced mild hyperthermia. PLoS One. 2012;7(4):e35509. doi:10.1371/journal.pone.0035509.
[33] Winter L, Oberacker E, Paul K, et al. Magnetic resonance thermometry: methodology, pitfalls and practical solutions. Int J Hyperthermia. 2016;32(1):63–75. doi:10.3109/02656736.2015.1108462.
[34] Partanen A, Yarmolenko PS, Viitala A, et al. Mild hyperthermia with magnetic resonance-guided high-intensity focused ultrasound for applications in drug delivery. Int J Hyperthermia. 2012;28(4):320–336. doi:10.3109/02656736.2012.680173.
[35] Anand A, Kaczkowski PJ. Monitoring formation of high intensity focused ultrasound (HIFU) induced lesions using backscattered ultrasound. Acoust Res Lett Online. 2004;5(3):88–94. doi:10.1121/1.1652131.
[36] Liu Y-D, Li Q, Zhou Z, et al. Adaptive ultrasound temperature imaging for monitoring radiofrequency ablation. PLoS One. 2017;12(8):e0182457. doi:10.1371/journal.pone.0182457.
[37] Ebbini ES, Simon C, Liu D. Real-time ultrasound thermography and thermometry [life sciences]. IEEE Signal Process Mag. 2018;35(2):166–174. doi:10.1109/MSP.2017.2773338.
[38] Duric N, Littrup P, Poulo L, et al. Detection of breast cancer with ultrasound tomography: first results with the Computed Ultrasound Risk Evaluation (CURE) prototype. Med Phys. 2007;34(2):773–785. doi:10.1118/1.2432161.
[39] Littrup PJ, Duric N, Sak M, et al. Multicenter study of whole breast stiffness imaging by ultrasound tomography (SoftVue) for characterization of breast tissues and masses (in eng). J Clin Med. 2021;10(23):5528. doi:10.3390/jcm10235528.
[40] Treeby BE, Cox BT. k-Wave: MATLAB toolbox for the simulation and reconstruction of photoacoustic wave fields. J Biomed Opt. 2010;15(2):021314–12. doi:10.1117/1.3360308.
[41] Fink M. Time-reversed acoustics. Sci Am. 1999;281(5):91–97. doi:10.1038/scientificamerican1199-91.
[42] Fink M, Montaldo G, Tanter M. Time-reversal acoustics in biomedical engineering. Annu Rev Biomed Eng. 2003;5(1):465–497. doi:10.1146/annurev.bioeng.5.040202.121630.
[43] Amador C, Aristizabal S, Greenleaf JF, et al. Effects of phase aberration on acoustic radiation force-based shear wave generation. In *2014 IEEE International Ultrasonics Symposium*; 2014. IEEE. p. 2316–2319.
[44] Ali R. Sound speed estimation and phase-aberration correction for medical ultrasound imaging [dissertation]. Stanford University; 2021. https://www.proquest.com/docview/2637956153?pq-origsite=gscholar&fromopenview=true&sourcetype=Dissertations%20&%20Theses.
[45] Ali R, Brevett T, Hyun D, et al. Distributed aberration correction techniques based on tomographic sound speed estimates (in eng). IEEE Trans Ultrason Ferroelectr Freq Control. 2022;69(5):1714–1726. doi:10.1109/tuffc.2022.3162836.
[46] Yeats E, Hall TL. Aberration correction in abdominal histotripsy. Int J Hyperthermia. 2023;40(1):2266594. doi:10.1080/02656736.2023.2266594.
[47] Huber PE, et al. A new noninvasive approach in breast cancer therapy using magnetic resonance imaging-guided focused ultrasound surgery. Cancer Res. 2001;61(23):8441–8447.

[48] Feng L, Shi X, Zhou F, et al. Evaluation of the acoustic radiation force imaging for predicting HIFU focus with in vitro and ex vivo experiments. Med Phys. 2023;50(9):5449–5459. doi:10.1002/mp.16565.

[49] Kim C, Yoon C, Park J-H, et al. Evaluation of ultrasound synthetic aperture imaging using bidirectional pixel-based focusing: preliminary phantom and in vivo breast study. IEEE Trans Biomed Eng. 2013;60(10):2716–2724. doi:10.1109/TBME.2013.2263310.

[50] Chen H, Han Y, Payen T, et al. Harmonic motion imaging in abdominal tumor detection and HIFU ablation monitoring: a feasibility study in a transgenic mouse model of pancreatic cancer. In *2014 IEEE International Ultrasonics Symposium*; 2014. IEEE. p. 923–926.

[51] Zhou X, Wang Y, Li Y, et al. Acoustic beam mapping for guiding HIFU therapy in vivo using sub-therapeutic sound pulse and passive beamforming. IEEE Trans Biomed Eng. 2021;69(5):1663–1673. doi:10.1109/TBME.2021.3126734.

[52] Bohndiek SE, Bodapati S, Van De Sompel D, et al. Development and application of stable phantoms for the evaluation of photoacoustic imaging instruments (in eng). PLoS One. 2013;8(9):e75533. doi:10.1371/journal.pone.0075533.

[53] Spirou GM, Oraevsky AA, Vitkin IA, et al. Optical and acoustic properties at 1064 nm of polyvinyl chloride-plastisol for use as a tissue phantom in biomedical optoacoustics (in eng). Phys Med Biol. 2005;50(14):N141–53. doi:10.1088/0031-9155/50/14/n01.

[54] Hungr N, Long JA, Beix V, et al. A realistic deformable prostate phantom for multimodal imaging and needle-insertion procedures (in eng). Med Phys. 2012;39(4):2031–2041. doi:10.1118/1.3692179.

[55] Nasoni RL, Bowen T, Connor WG, et al. In vivo temperature dependence of ultrasound speed in tissue and its application to noninvasive temperature monitoring. Ultrason Imaging. 1979;1(1):34–43. doi:10.1016/0161-7346(79)90004-X.

[56] Varghese T, Zagzebski JA, Chen Q, et al. Ultrasound monitoring of temperature change during radiofrequency ablation: preliminary in-vivo results. Ultrasound Med Biol. 2002;28(3):321–329. doi:10.1016/s0301-5629(01)00519-1.

[57] Arthur RM, Straube WL, Trobaugh JW, et al. Non-invasive estimation of hyperthermia temperatures with ultrasound. Int J Hyperthermia. 2005;21(6):589–600. doi:10.1080/02656730500159103.

[58] Del Grosso V, Mader C. Speed of sound in pure water. J Acoust Soc Am. 1972;52(5B):1442–1446. doi:10.1121/1.1913258.

[59] Bilaniuk N, Wong GS. Speed of sound in pure water as a function of temperature. J Acoust Soc Am. 1993;93(3):1609–1612. doi:10.1121/1.406819.

[60] Wilson CB, Lammertsma AA, McKenzie CG, et al. Measurements of blood flow and exchanging water space in breast tumors using positron emission tomography: a rapid and noninvasive dynamic method (in eng). Cancer Res. 1992;52(6):1592–1597.

[61] Vaupel P, Piazena H. Strong correlation between specific heat capacity and water content in human tissues suggests preferred heat deposition in malignant tumors upon electromagnetic irradiation (in eng). Int J Hyperthermia. 2022;39(1):987–997. doi:10.1080/02656736.2022.2067596.

[62] Cook JR, Bouchard RR, Emelianov SY. Tissue-mimicking phantoms for photoacoustic and ultrasonic imaging (in eng). Biomed Opt Express. 2011;2(11):3193–3206. doi:10.1364/boe.2.003193.

[63] Farrer AI, Odéen H, de Bever J, et al. Characterization and evaluation of tissue-mimicking gelatin phantoms for use with MRgFUS. J Ther Ultrasound. 2015;3(1):9. doi:10.1186/s40349-015-0030-y.

[64] Ali R, Mitcham TM, Brevett T, et al. 2-D slicewise waveform inversion of sound speed and acoustic attenuation for ring array ultrasound tomography based on a block LU solver. IEEE Trans Med Imaging. 2024;PP:1–1. doi:10.1109/TMI.2024.3383816.

[65] Sandhu G, Li C, Roy O, et al. Frequency domain ultrasound waveform tomography: breast imaging using a ring transducer. Phys Med Biol. 2015;60(14):5381–5398. doi:10.1088/0031-9155/60/14/5381.

[66] Meltzer RS. Food and Drug Administration ultrasound device regulation: the output display standard, the "mechanical index," and ultrasound safety. J Am Soc Echocardiogr. 1996; 9(2):216–220. doi:10.1016/S0894-7317(96)90035-8.

[67] Priester MI, Curto S, van Rhoon GC, et al. External Basic Hyperthermia Devices for Preclinical Studies in Small Animals (in eng). Cancers (Basel). 2021;13(18):4628. doi:10.3390/cancers13184628.

[68] Partanen A, Tillander M, Yarmolenko PS, et al. Reduction of peak acoustic pressure and shaping of heated region by use of multifoci sonications in MR-guided high-intensity focused ultrasound mediated mild hyperthermia. Med Phys. 2013;40(1):013301. doi:10.1118/1.4769116.

[69] Osmanski BF, Montaldo G, Tanter M, et al. Aberration correction by time reversal of moving speckle noise. IEEE Trans Ultrason Ferroelectr Freq Control. 2012;59(7):1575–1583. doi:10.1109/TUFFC.2012.2357.

[70] Ghoshal G, Luchies AC, Blue JP, et al. Temperature dependent ultrasonic characterization of biological media (in eng). J Acoust Soc Am. 2011;130(4):2203–2211. doi:10.1121/1.3626162.